Memoirs of the Faculty of Engineering, Kyushu University, Vol. 63, No. 3, September 2003

# Development of Pulsatile Flow Experiment System and PIV Measurement in an Elastic Tube

by

Takashi EGUCHI*, Satoshi WATANABE**, Hisasada TAKAHARA***
and Akinori FURUKAWA****

(Received July 8, 2003)

**Abstract**

The heart diseases are one of the major causes of death in recent years. Most of them are related to the atherosclerosis of coronary artery, whereas the mechanism of atherosclerosis is still unknown and the only known is that the atherosclerosis occurs under the influence of blood flow and the wall stresses on vessel walls. In the present study, in order to obtain the information of unsteady flow in the blood vessels, the flow structures of pulsatile flows in an elastic tube modeled as a blood vessel are investigated. Firstly, to validate our PIV (Particle Image Velocimetry) measurement technique, we apply it to sinusoidal flows with no net flow rate in a rigid straight tube, for which the exact solution with low Reynolds number exists. Then, two types of imitated blood flow in arteries are simulated in a rigid and an elastic straight tubes, and the results are compared together with the numerical simulation, which is also constructed in the present study, using SMAC type fractional step method with ALE (arbitrary Lagrangian and Euler) moving grids treatment. Finally, the effects of elastic boundaries on local flows as well as the wall shear stresses are discussed.

**Keywords:** Pulsatile flow, Arterial blood flow, Particle image velocimetry, Numerical simulation, Rigid and elastic vessels

*Graduate Student of Doctor Course, Department of Mechanical Engineering Science
**Associate Professor, Department of Mechanical Engineering Science
***Research Associate, Department of Mechanical Engineering Science
****Professor, Department of Mechanical Engineering Science

## 1. Introduction

The heart diseases are one of the major causes of death in recent years. The most severe one, the acute myocardial infarction, is known to occur due to the necrosis of the cardiac muscles caused by the atherosclerosis of coronary artery, which supplies nutrition into the cardiac muscles. The mechanism of atherosclerosis, i.e. inception, growth and break down of atherosclerotic lesion is still unknown, and the only known is that the atherosclerosis occurs under the influence of blood flow and the wall stresses on vessel walls.

Recently, many researchers have begun to study the mechanism of atherosclerosis in the fluid dynamics sense. Many of them[1)-2)] are based on the computational fluid dynamics (CFD), which is developing rapidly, and have provided the detail descriptions of unsteady flow structures in modeled blood vessels. However, there seems not to be sufficient data for the validation of CFD results, and most of experimental works done before are limited to steady[3)] or pulsatile[4)] flows in model vessels with rigid wall, wheres the interaction between the elastic motion of vessels and the pulsatile blood flow produced by the real heart might play an important role in the atherosclerosis.

We have developed a pump system consisting of a constant flow pump, three sinusoidal wave plungers and a rectified sinusoidal wave pump with delivery and suction valves[5)], which have been found to be able to produce any periodic flows including the imitated pulsatile blood flow in arteries. In the present study, with the aid of the above pump system, the flow structures of pulsatile flows in an elastic tube modeled as a blood vessel are investigated. Firstly, in order to validate our PIV (Particle Image Velocimetry)[6)] measurement technique, we apply it to sinusoidal flows with no net flow rate in a rigid tube, for which the exact solution with low Reynolds number exists[7),8)]. Then, two types of imitated blood flow in arteries are simulated in a rigid/elastic tubes, and the results are compared together with the numerical simulation, which is also constructed in the present study, using SMAC type fractional step method with ALE (arbitrary Lagrangian and Euler) moving grids treatment. Finally, the effects of elastic boundaries on local flows as well as the wall shear stresses are discussed.

## 2. Experimental Procedure

### 2.1 Experimental apparatus with pulsatory flow pump system

The experimental apparatus with the present pulsatory flow pump system is shown in **Figs. 1 (a)** and **(b)**. The test section, which is a rigid/elastic straight tube as shown in **Fig. 1 (b)**, is vertically attached downstream of the pulsatory flow pump system. Volumetric flow rates, $Q_{in}$ and $Q_{out}$, and wall pressures, $p_{in}$ and $p_{out}$, upstream and downstream of the test section are measured respectively by individually installed magnetic flow rate meters and pressure transducers. Because the pressure does not differ between upstream and downstream of the test section with the small inertia and resistance in the test tubes, we define $\Delta p = p_{out} - p_0$ for representing the reference pressure difference between inside and outside of the tested tube, where $p_0$ denotes the pressure outside of the test tubes. The open tank with sufficiently large cross-sectional area is installed in order to absorb the volume change of the elastic tube.

The pulsatory flow pump system used in the present study was a modified version of the one developed by Kiyose et al.[5)] as illustrated by **Fig. 1 (a)**. The pump system consists of a constant flow pump, five sinusoidal wave plungers and a rectified sinusoidal wave plungers with delivery and suction valves, which have been found to be able to simulate many types of periodic flows. In the present study, we test three types of waveforms as **(a)** sinusoidal waveform with no net flow rate,

**(b)** pulsatile waveform of typical normal arterial blood flow (Type A), and (c) pulsatile waveform of typical arterial blood flow with the arteriosclerosis (Type B), as shown in **Figs. 2 (a)-(c)**.

Two test tubes with a rigid and an elastic wall are used in the present study. The rigid tube is made of an acrylic resin with a part of the surface flattened for the flow visualization to avoid the deformation of images as much as possible; it is still needed to modify the images due to the difference in the refractive indices with different materials. The elastic tube is made of transparent silicon,

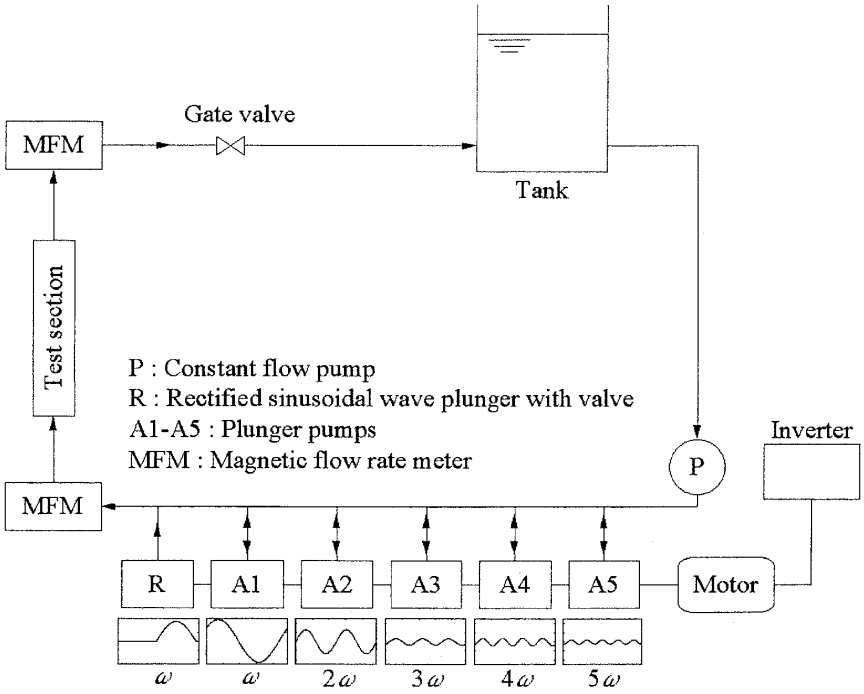


(a) Experimental apparatus

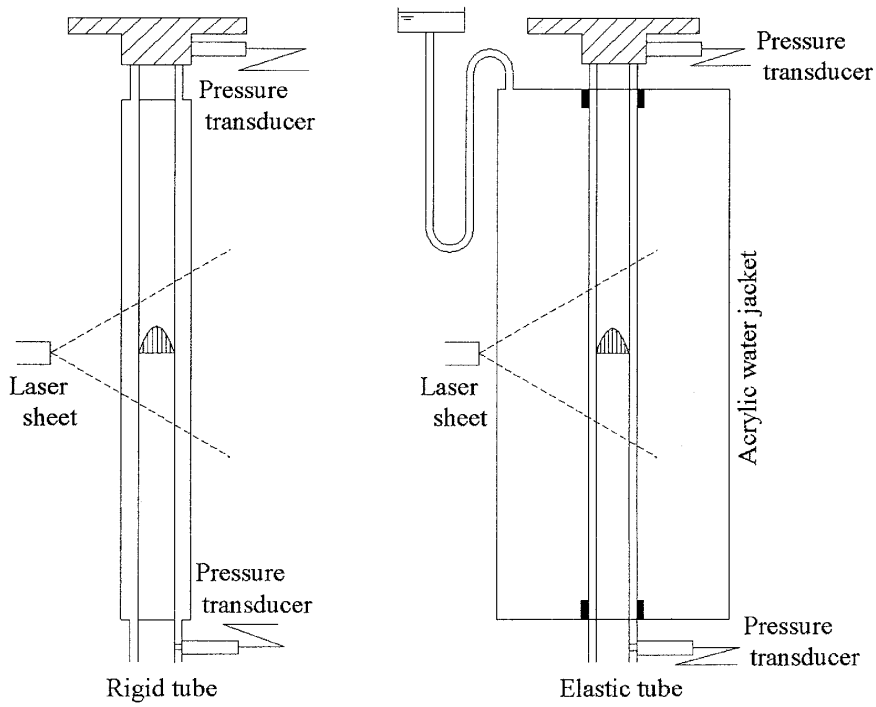


(b) Test section

**Fig. 1** Experimental apparatus and test section

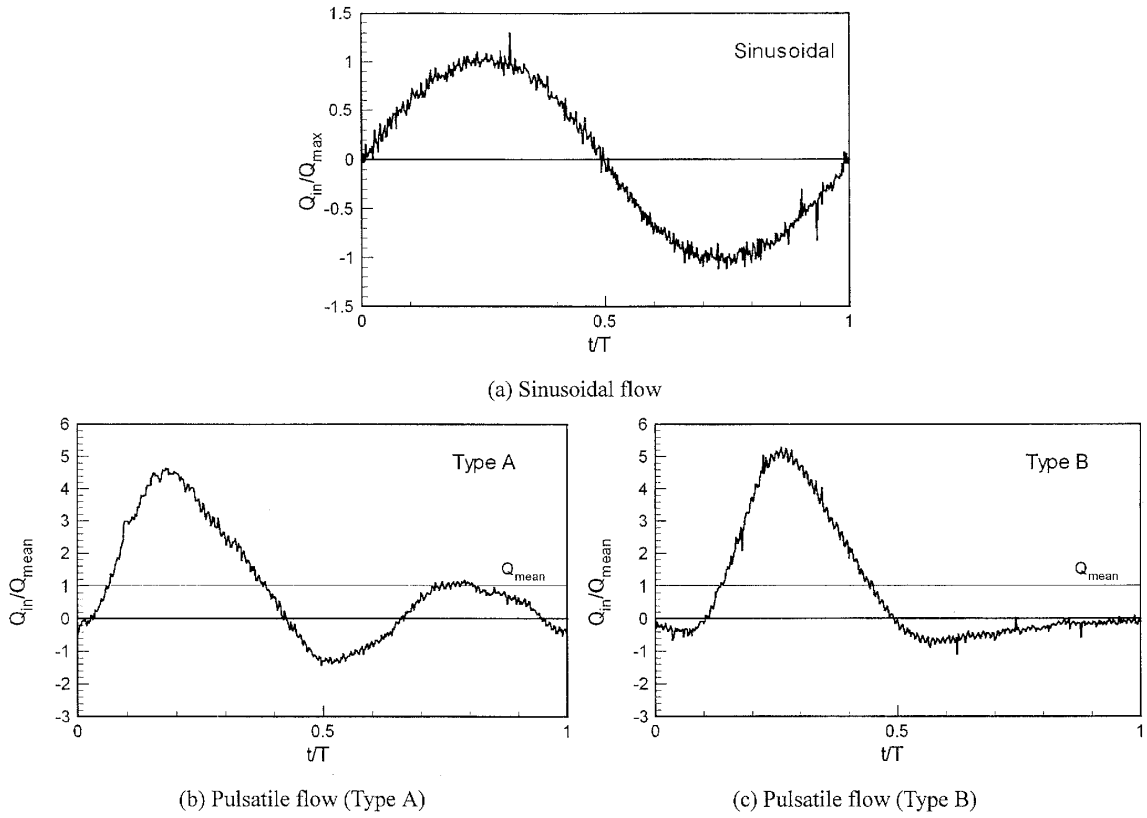


(a) Sinusoidal flow

(b) Pulsatile flow (Type A)

(c) Pulsatile flow (Type B)

**Fig. 2** Waveforms of tested pulsatile flow

**Table 1** Mechanical characteristics of elastic tube

| | |
|---|---|
| Density [kg/m$^3$] | $2.21\times10^3$ |
| Young's modulus [N/m$^2$] | $1.13\times10^6$ |
| Poisson's ratio [−] | $4.03\times10^{-1}$ |

whose material characteristics are summarized in **Table 1**. The thickness of the test elastic tube is 2.5 mm. An acrylic water jacket is used to avoid the deformation of images. The change of refractive index of elastic tube due to its deformation is found to be negligible within the range of pressure difference between inside and outside of the tube applied in the present study.

## 2.2 PIV technique

In order to obtain the unsteady velocity profiles during the periodic flows in the elastic/rigid test tubes, two-dimensional cross-correlation PIV technique is applied. The nylon 12 particles with the diameter of approximately 50 μm and the specific gravity of 1.03 are used as seeding particles. The Ar laser sheet with the thickness of 0.5 mm is used as a light source and the images are recorded by a CCD video camera and stored as digital images in PC, where the post-process with cross correlation PIV technique is made. Usually, PIV measurement of unsteady flow requires a high-speed video camera or a double-pulse laser controlled by AOM (Acoustic Optic Modulator) to obtain the continuous images with the sufficiently small time delay, whereas, in the present study, we use neither because of large periodicity of the applied pulsatile flow.

The recorded analog images are converted to the digital images by a video capture board and stored in PC, which contains 240×200 pixels inside of the tube with the diameter of $D$ =20 mm in the case with the rigid tube. Then, all the video images are converted into grey-scaled images for

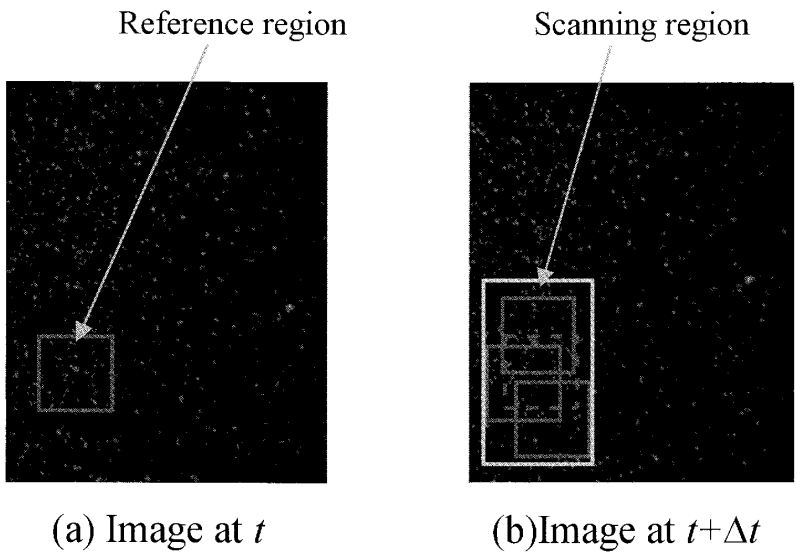


**Fig. 3** Two consecutive images used for PIV. Reference and scanning regions are indicated.

the two-frame cross-correlation PIV post-processing.

To obtain the velocity vectors, cross-correlation coefficients are calculated by comparing the gray level between two consecutive images with the time interval of 0.033 s. The main principle of the algorithm is as follows:

(I) Take the small reference region 17×17 around the point where the velocity vector is being measured. (See, **Fig. 3 (a)**.)

(II) Define the scanning region 10×60 as shown in **Fig. 3 (b)**, and calculate the cross-correlation coefficients of the grey level between the reference region in the first image and any regions in the scanning region in the second image.

(III) Find the location of the reference region with the maximum cross-correlation coefficient, from which we can calculate the displacement of the fluid particle within the time interval of the two frames, and then we obtain the velocity vector.

Repeating the above procedure (I)-(III), we obtain the velocity vector distributions allover the images, whereas, in the present study, we focus on the velocity vector distribution at the mid-length location of the rigid/elastic test tube; the length of the tested tubes is 300 mm in the present study.

### 2.3 Experimental conditions

The typical condition of peripheral artery is regarded approximately as the inner diameter of $D_a$ =10 mm, the pulse rate of $f_a$ =1 Hz, the maximum peak flow rate of $Q_{amax}$ =1.8 l/min, and kinematic viscosity of $\nu_a$ =4.0×10$^{-6}$ m$^2$/s. For the fluid dynamic and hemodynamic similarity, the following two non-dimensional parameters, Reynolds and Womersley numbers, must be the same for the real and simulated flows.

$$\mathrm{Re} = \frac{U_{max} D}{\nu} = \frac{4Q_{max}}{\pi D \nu} = 955$$

$$\alpha = \frac{D}{2}\sqrt{\frac{\omega}{\nu}} = 6.27$$

Both the test rigid and elastic tubes have the diameter of $D$ =20 mm, which yields approximately to the following experimental conditions;

Pulse frequency: $f$ =1/16 Hz / Periodicity: $T$ =16 s

Maximum peak flow rate: $Q_{max}$ =800-1000 ml/min

## 3. Numerical Analysis

### 3.1 Fundamental equations

The Navier-Stokes equations described in the cylindrical coordinates are solved using SMAC-like fractional step method in combination with ALE (Arbitary Lagrangean and Eulerian) moving boundary treatment. Under the assumption of axisymmetric flow with no swirl components, the fundamental equations solved here can be written as;

$$\frac{\partial u}{\partial x}-\frac{r^*}{R}\frac{\partial R}{\partial x}\frac{\partial u}{\partial r^*}+\frac{R_0}{R}\frac{1}{r^*}\frac{\partial r^* v_r}{\partial r^*}=0 \tag{1}$$

$$\begin{aligned}&\frac{\partial u}{\partial t}+\frac{\partial u^2}{\partial x}-\frac{r^*}{R}\frac{\partial R}{\partial x}\frac{\partial u^2}{\partial r^*}+\frac{R_0}{R}\frac{1}{r^*}\frac{\partial r^* u v_r}{\partial r^*}=-\frac{1}{\rho}\left(\frac{\partial p}{\partial x}-\frac{r^*}{R}\frac{\partial R}{\partial x}\frac{\partial p}{\partial r^*}\right)\\&+\nu\frac{\partial}{\partial x}\left(\frac{\partial u}{\partial x}-\frac{r^*}{R}\frac{\partial R}{\partial x}\frac{\partial u}{\partial r^*}\right)-\nu\frac{r^*}{R}\frac{\partial R}{\partial x}\frac{\partial}{\partial r^*}\left(\frac{\partial u}{\partial x}-\frac{r^*}{R}\frac{\partial R}{\partial x}\frac{\partial u}{\partial r^*}\right)\\&+\nu\left(\frac{R_0}{R}\right)^2\frac{1}{r^*}\frac{\partial}{\partial r^*}\left(r^*\frac{\partial u}{\partial r^*}\right)\end{aligned} \tag{2}$$

$$\begin{aligned}&\frac{\partial v_r}{\partial t}+\frac{\partial u v_r}{\partial x}-\frac{r^*}{R}\frac{\partial R}{\partial x}\frac{\partial u v_r}{\partial r^*}+\frac{R_0}{R}\frac{1}{r^*}\frac{\partial r^* v_r^2}{\partial r^*}=-\frac{1}{\rho}\frac{R_0}{R}\frac{\partial p}{\partial r^*}\\&+\nu\frac{\partial}{\partial x}\left(\frac{\partial v}{\partial x}-\frac{r^*}{R}\frac{\partial R}{\partial x}\frac{\partial v_r}{\partial r^*}\right)-\nu\frac{r^*}{R}\frac{\partial R}{\partial x}\frac{\partial}{\partial r^*}\left(\frac{\partial v_r}{\partial x}-\frac{r^*}{R}\frac{\partial R}{\partial x}\frac{\partial v_r}{\partial r^*}\right)\\&+\nu\left(\frac{R_0}{R}\right)^2\frac{1}{r^*}\frac{\partial}{\partial r^*}\left(r^*\frac{\partial v_r}{\partial r^*}\right)+\nu\left(\frac{R_0}{R}\right)^2\frac{v_r}{r^{*2}}\end{aligned} \tag{3}$$

where $R$ and $R_0$ respectively denote the temporal and equilibrium radii of the tube, $\rho$ density, and $\nu$ dynamic viscosity of working fluid. The radial coordinate which stretches with the movement of the elastic wall is defined as $r^* = r\,(R_0/R)$, and the above equations are solved in this system.

Assuming that the elastic tube expand and shrink purely in the radial direction, non-slip wall boundary condition yields to the following form;

$$u=0, \quad v_r=\partial R/\partial t \qquad \text{at } r=R\ (r^*=R_0) \tag{4}$$

which needs the temporal radius of the tube. This is obtained by solving the following equation based on the membrane theory with the small thickness of the wall shell;

$$\frac{\partial^2}{\partial x^2}\left[\frac{Eh}{12\left(1-\nu_p^2\right)}\frac{\partial^2 R}{\partial x^2}\right]+\frac{Eh}{R_0^2}R=\Delta p \tag{5}$$

where $\Delta p$ is the reference pressure difference defined before as $\Delta p = p_{out}-p_0$. Generally, the local wall pressure must be used for the pressure difference in the right hand side of the above equation, whereas the reference pressure difference is used here because the pressure deviation due to the local flow is much smaller than the temporal system pressure change due to pulsatory flow in the present study. We have confirmed that this simplification gives good approximation by comparing the result of full computation using local pressure difference in **Eq. (5)**.

The other boundary conditions applied are as follows.

At the center of axis, radial velocity component must diminish because of the assumption of axisymmetric flow. The inflow volumetric flow rate $Q_{in}$ is given at the inlet. The corresponding velocity profile is calculated under the assumption of $\partial u/\partial x = 0$ in the rigid tube, and applied for the

inlet boundary condition. A static pressure is given at the outlet boundary.

### 3.2 Numerical procedure

In the present study, the motion of the elastic wall of the tube and the fluid flow inside are coupled and simulated by solving the above-described equations. The all spatial derivative terms are evaluated by 2nd order central finite difference method, and the time integration is done by a SMAC like fractional step method on the 1st order basis. Overall numerical procedure can be summarized as follows;

(i) Calculate the inflow velocity distribution $u_{in}^{t+\Delta t}$ which is needed for the inlet boundary condition.

(ii) Calculate deformation of elastic tube, i.e. the temporal radius distribution $R^{t+\Delta t}$, from **Eq. (5)** with the given reference pressure.

(iii) Estimate the velocity predictions, $(u^p, v_r^p)$, by time integrating the **Eqs. (2)** and **(3)** using the values at time $t$. Note that these predictions do not satisfy the continuity **equation (1)**.

(iv) Solve the Poisson's equation on the potential correction term $\phi$, to make the velocity components at $t = t + \Delta t$ satisfy the continuity **equation (1)**.

(v) Correct the velocity components and obtain the pressure from the potential correction term $\phi$.

(vi) Return to the step (i) and proceed to the next time step.

The computational domain consists of an inlet rigid tube part with the length of 20 mm and the radius of 10 mm, the test elastic tube part with the length of 300 mm, and an outlet rigid tube part with the length of 20 mm and the radius of 10 mm. A staggered grid system with the mesh size of $n_x \times n_r = 340 \times 20$ and the constant $\Delta x$ and $\Delta r^*$ of 1 mm is used in the present study. The computational results with this grid system have been confirmed not to alter from those of the computation with the finer mesh in some test cases.

## 4. Results and Discussions

### 4.1 Validation of PIV technique with exact solution

In order to validate the present PIV measurement technique, we apply it for a purely sinusoidal periodic flow with no net flow rate in the rigid tube. The result is compared with the exact solution, which can be found in some textbooks (see, for example, White[6] and Zamir[7].)

**Figure 4 (a)** shows instantaneous axial velocity distributions in one cycle of sinusoidal flow rate fluctuation, where the velocities normalized by the area-averaged velocity at the maximum flow rate, $v_{max} = 4Q_{max}/\pi D^2$, are plotted. The maximum flow rate and the frequency are $Q_{max} = 0.80$ l/min and $f = 1/16$ Hz, respectively. We can see that the measured velocities by the present PIV agree fairly well with those of the exact solution. In **Fig. 4 (b)**, the volumetric flow rate, $Q_{est}$, estimated by the integration of the velocity distributions obtained by PIV in **Fig. 4 (a)** is plotted for one cycle. The estimate agrees with the measured value of the magnetic flow meter plotted with a solid line in **Fig. 4 (b)**.

Based on the above obtained results, we conclude that the present PIV measurement technique is capable for the velocity measurement in unsteady periodic flows. Next, we proceed for the PIV measurement of unsteady flows in an elastic tube.

### 4.2 PIV technique in an elastic tube

Now, we apply the present PIV technique for pulsatory arterial flow in the elastic tube. Numerical simulation is also done using the experimentally obtained inflow volumetric flow rate, $Q_{in}$, and the reference pressure difference, $\Delta p / \rho g$.

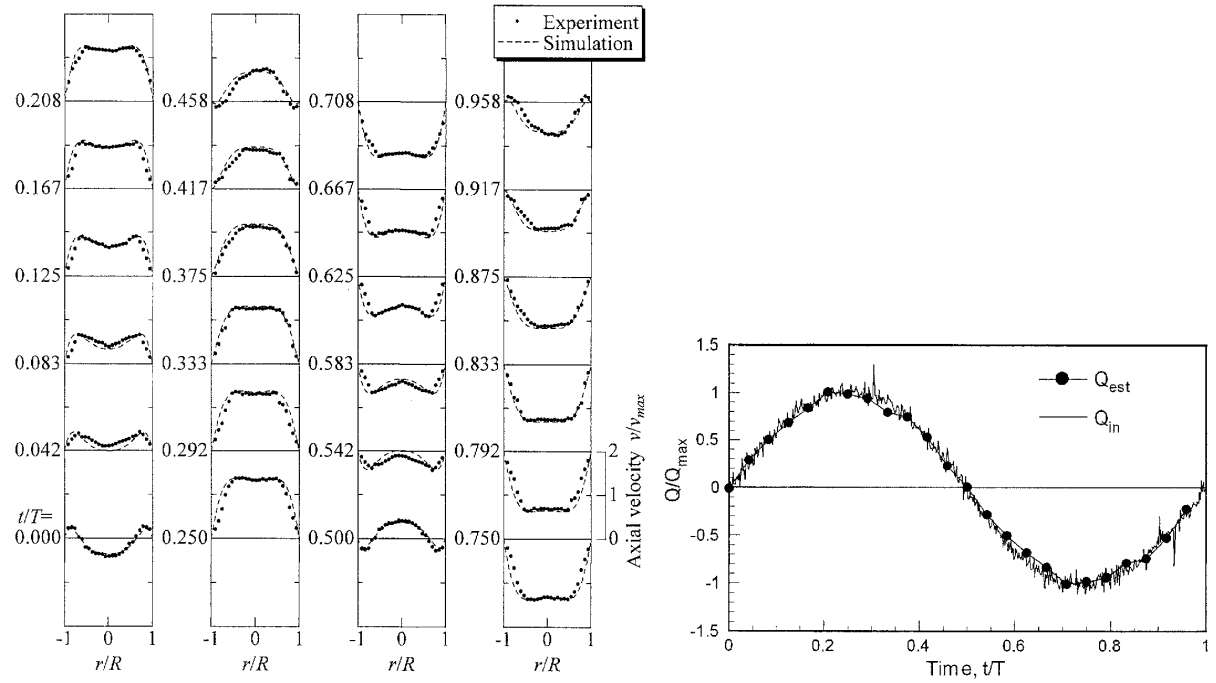


(a) Instantaneous velocity profiles (b)Flow rate fluctuation

**Fig. 4** Velocity distributions in rigid tube in the case with sinusoidal flow with no net flow rate. Estimates of flow rate from velocity profiles are compared with the measured flow rate.

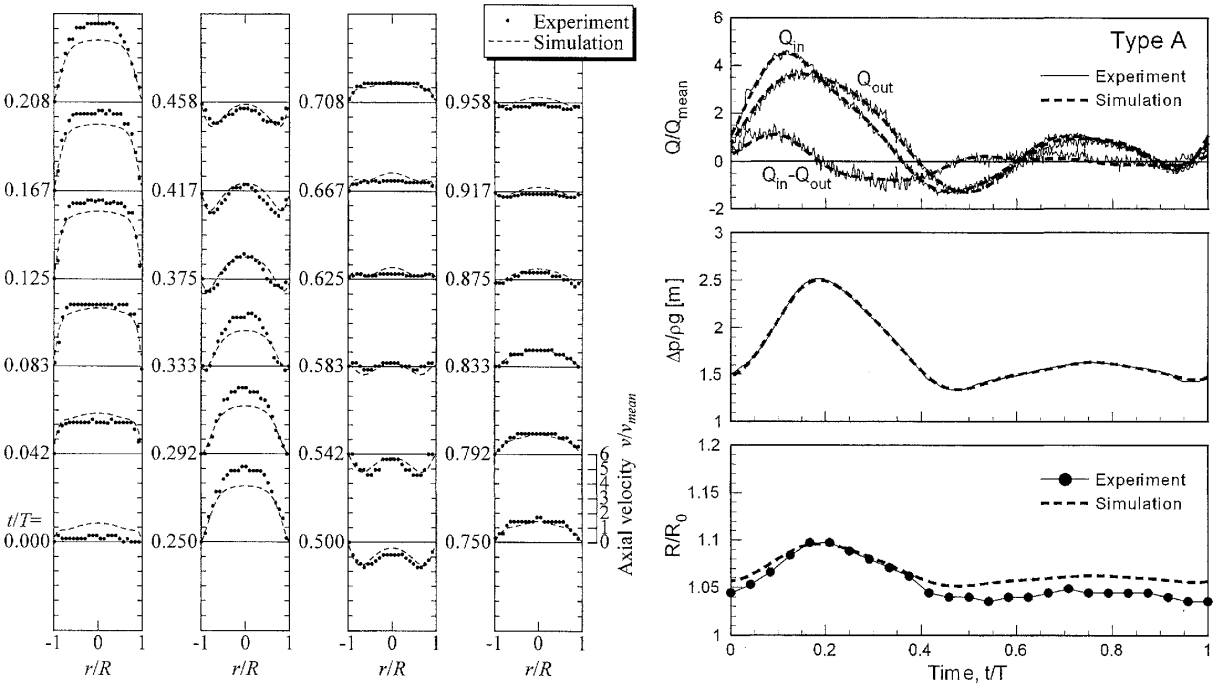


(a) Instantaneous velocity distributions (b) Time histories of variables

**Fig. 5** Measured and calculated temporal velocity distributions and time histories of inflow and outflow volumetric flow rates, flow rate difference, reference pressure difference, and radius of the tube in the case with pulsatile flow with waveform of Type A.

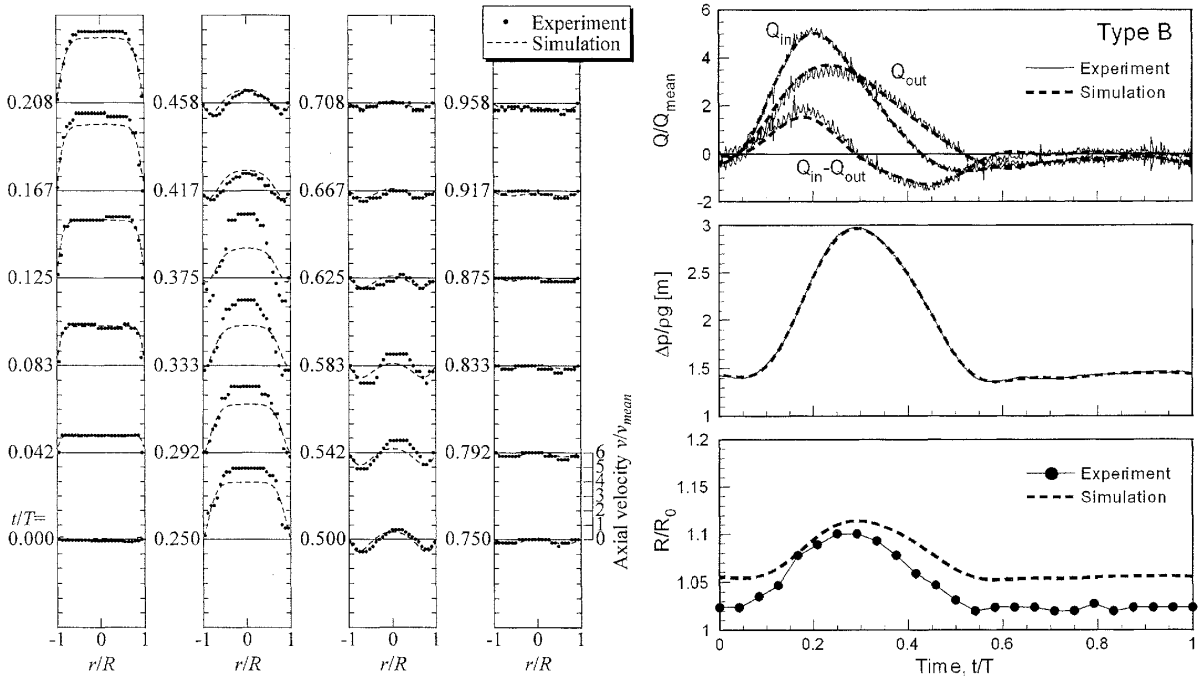


(a) Instantaneous velocity distributions

(b) Time histories of variables

**Fig. 6** Measured and calculated temporal velocity distributions and time histories of inflow and outflow volumetric flow rates, flow rate difference, reference pressure difference, and radius of the tube in the case with pulsatile flow with waveform of Type B.

**Figure 5** shows the results for the case with Type A, which is a typical waveform of normal arterial blood flow. The time-averaged flow rate and the frequency are $Q_{mean}$ =0.211 l/min and $f$ = 1/16 Hz, respectively. **Figure 5 (a)** shows instantaneous axial velocity distributions in one cycle, where the velocities normalized by the mean velocity of time-averaged flow rate, $v_{mean} = 4Q_{mean}/\pi D^2$, are plotted with closed circles. The radial location is normarized by the temporal radius of elastic tube as $r/R\ (t)$. Results of numerical simulation are also plotted with dashed lines. We can see that the measured velocities by the present PIV agree fairly well with those of the numerical simulation, except that the in-negligible discrepancies can be seen during $t/T$ =0.25-0.375, in which the measured velocity is larger especially around the center of the tube. **Figure 5 (b)** shows time histories of the inflow and outflow flow rates, $Q_{in}$ and $Q_{out}$, the flow rate difference, $Q_{in} - Q_{out}$, the reference pressure difference, $\Delta p/\rho g$ and the radius of the tube, $R/R_0$. A good agreement between the experiment and the numerical simulation can be seen for those values. Thus, the reason why we have in-negligible discrepancies of velocity distributions during $t/T$ =0.25-0.375 is unknown, but one possible explanation is that the elastic tube does not shrink axisymmetrically; this duration corresponds to the shrinking period of the elastic tube. To examine this hypothesis, we need further investigation for the motion of elastic wall of the vessel in multi-dimensions.

**Figure 6** shows the results for the case with Type B, which is a typical waveform of arterial blood flow with arteriosclerosis. The time-averaged flow rate and the frequency are $Q_{mean}$ =0.205 l/min and $f$ = 1/16 Hz, respectively. A good agreement between the experiment and the numerical simulation can be also found in this case, except that the in-negligible discrepancies can be seen in the shrinking period of the elastic tube, just as we have observed in the case with Type A.

From the above results, the present PIV technique seems to be capable for the cases even with the unsteady flows in the elastic tube under the conditions we examined in this experimental study. We should note that the validation was made just for the axisymmetric flow with the axisymmetric motion of elastic wall of the vessel. The further validation with various conditions is favorable for

more reliability of the present PIV technique.

### 4.3 Effects of elasticity of vessel wall

**Figure 7 (a)** shows the comparisons of PIV measurement between in the rigid tube and in the elastic tube for the case with the pulsatile flow with Type A waveform. **Figure 7 (b)** shows the time histories of the estimated flow rates, $Q_{elastic}$ and $Q_{rigid}$, which are obtained by integrating the measured velocity profiles shown in **Fig. 7 (a)**. The radius of the elastic tube is also plotted in the figure. The apparent difference of the flow patterns between in the elastic and rigid tubes can be seen espe-

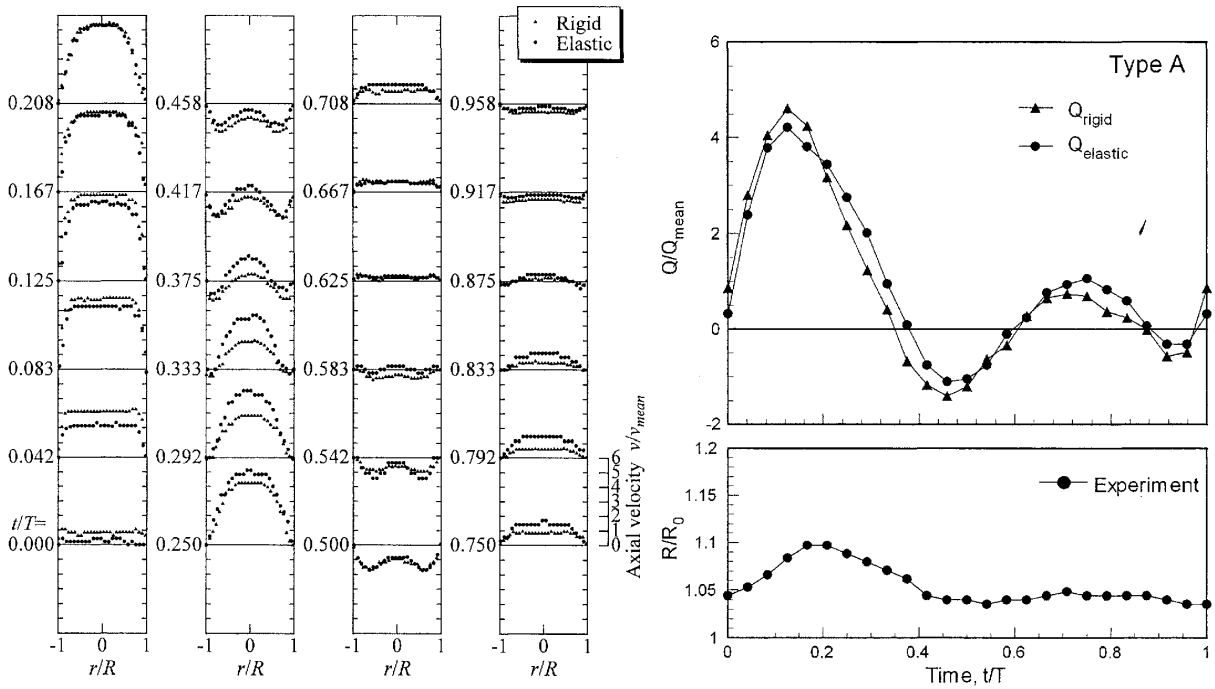


(a) Instantaneous velocity distributions (b) Time histories of variables

**Fig. 7** Comparisons of experimental results between rigid and elastic tube flows with Type A pulsatile flow rate waveform

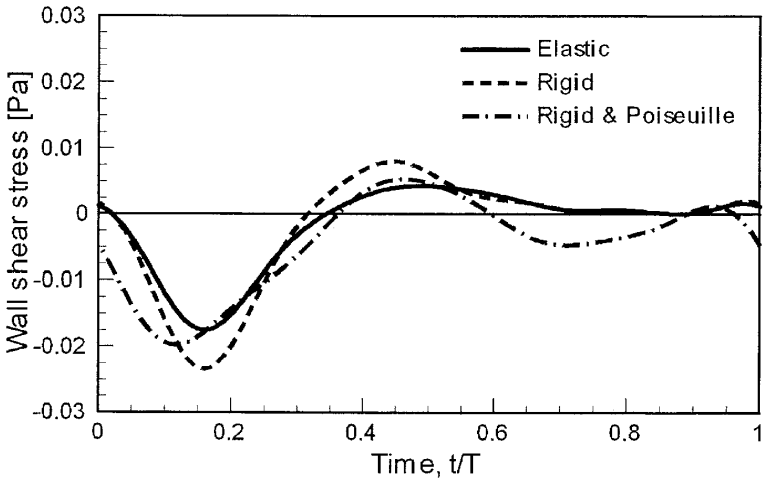


**Fig. 8** Time histories of numerical wall shear stress for pulsatile flow with Type I at the mid-length of rigid and elastic tubes. The estimate of wall shear stress under the assumption of Poiseuille flow in rigid tube is also plotted.

cially around $t/T=0.042$ and 0.333; which respectively corresponds to the moments with the maximum growth and shrink rates of the elastic tube as you can see from the temporal radius shown in **Fig. 7 (b)**. At those moments, the net flow rate differs from the inlet flow rate, i.e. flow rate in the case with rigid tube, resulting in the deviation of flow pattern from that in the rigid tube. It can be also seen that the deviation of flow pattern is more remarkable around $t/T=0.333$ than around $t/T=0.042$. We are supposing that this is due to the axi-asymmetric shrink of the elastic tube, recalling the fact that, in the shrinking period of the elastic tube, the velocity profiles measured by PIV differ from those obtained by numerical simulation as shown in **Fig. 5 (a)** and **6 (a)**.

**Figure 8** shows the time histories of wall shear stress obtained by numerical simulation for the pulsatile flow with Type A waveform in the rigid and elastic tube. The estimate of the shear stress assuming the laminar Poiseuille flow in a rigid tube is also plotted in the figure. We can see that the elasticity of the vessel wall reduces the fluctuation of wall shear stress as well as the time-averaged shear stress, which is a favorable condition to avoid the atherosclerosis. The assumption of laminar Poiseuille flow is apparently insufficient for the estimation of wall shear stress.

## 5. Conclusions

In the present study, the PIV (Particle Image Velocimetry) measurement technique and numerical scheme using SMAC type fractional step method with ALE (arbitrary Lagrangian and Euler) moving grids treatment, both of which are capable for analyses of the unsteady flows in elastic tubes, are developed, and the flow structures of two types of typical pulsatile blood flows in a rigid and an elastic tubes are investigated. The obtained results are summarized as follows.

(1) The present PIV technique is validated by comparing the results with the exact solution in the case with the rigid tube, and with the numerical analysis in the case with the elastic tube. This also indicates that the present numerical analysis can simulate the unsteady flow in elastic tubes despite of the very simple coupling between the fluid dynamics and the elastic dynamics of thin shell vessel wall.

(2) The apparent difference of the flow patterns between in the elastic and rigid tubes can be seen especially around the moments with the maximum growth and shrink rates of the elastic tube. At those moments, the volumetric flow rate differs from the that of the inflow, which makes the flow pattern deviated from that in the rigid tube.

(3) The elasticity of the vessel wall reduces the fluctuation of wall shear stress as well as the time-averaged shear stress. This is a favorable condition for the avoidance of the atherosclerosis.

## 6. Acknowledgement

The authors would like to thank to the graduate students, Mr. Kazumichi Matsuishi and Ms. Ayano Matsushima in Kyushu University, who made their large efforts to accomplish the present experimental work.

## References

1) Oshima, M., Torii, R., Kobayashi, T., Taniguchi, N. and Takagi, K.: Finite Element Simulation of Blood Flow in the Cerebral Artery, *Compt. Methods Appl. Mech. Eng.,* 131, (2001), 661.

2) Mori, D. and Yamaguchi, T.: Computational Fluid Dynamics Simulation of the Blood Flow in the Human Aortic Arch (combined Effects of the Torsion of the Arch and its Branches on Flows), *Proc. the 5th jSme-KSme Fluids Eng. Conf.,* Nagoya, Japan, (2002).

3) Yamaguchi, R., Kudo, S., Amagai, H. and Hayase, T.: Flow Structure and Periodic Oscillations

Induced in Right-Angle Branches During Laminar, Steady Flow, *Proc. the 5th jSme-KSme Fluids Eng. Conf.,* Nagoya, Japan, (2002).

4) Suh, S.-H., Cho, M.-T. and Roh, H.-W.: Hemodynamic Studies using Flow Visualization Techniques, *Proc. Japan-Korea Joint PIV Seminar,* Fukuoka, Japan, (2002).
5) Kiyose, T., Kusaba, A., Kamori, K., Inokuchi, K, Takamatsu, Y. and Takahara, H.: Development of Pump System for Experimental Model Simulation of Blood Flow in Peripheral Artery, *Fukuoka Acta Med.,* 68-2, (1977), 86.
6) Adrian, R. J.: Particle-Imaging Technologies for Fluid Mechanics, *Annu. Rev. Fluid. Mech.,* 23, (1991), 261.
7) White, F. M.: Viscous Fluid Flow, McGraw Hill, (1974).
8) Zanir, M.: The Physics of Pulsatile Flow, Biological Physics Series, Springer-Verlag, (2000).